AIAA JOURNAL
Vol. 46, No. 8, August 2008

Experimental Study of the Far Field of Incompressible Swirling Jets

Abolfazl Shiri* and William K. George†
Chalmers University of Technology, 412 96 Götebory, Sweden
and
Jonathan W. Naughton‡
University of Wyoming, Laramie, Wyoming 82071

DOI: 10.2514/1.32954

The far field of an incompressible swirling jet has been studied using two-component laser Doppler anemometry. Three pairs of symmetric injectors were used to produce weak-to-moderate swirling jets. Velocity profiles of the mean and fluctuating streamwise and azimuthal velocity components were measured in jets with two swirl numbers ($S = 0.15$ and 0.25) at axial locations up to 50 jet exit diameters. The velocity and turbulence intensity profiles, centerline decay, and growth rates for the various swirling jets have been compared with those obtained in the same facility without swirl ($S = 0$). Like the previous observations for the near jet, there was no observable effect on the properly scaled far jet for the $S = 0.15$ case. The results were virtually identical to the nonswirling jet. For the $S = 0.25$ case, the only statistically significant effect was a shift in the virtual origin (from $x/D_* = 0.75$ to -2.9). The recent predictions of equilibrium similarity theory were found to be in excellent agreement with the experimental results. In particular, the mean azimuthal component of velocity falls off as the inverse square of the downstream distance. By contrast, the mean streamwise velocity and turbulence intensities fall off with the inverse of the downstream distance. As a consequence, the mean azimuthal equation uncouples from the rest, and so the asymptotic swirling jet behaves like the nonswirling jet.

Nomenclature

A, B_u, C	=	growth rate constants for self-preserving axisymmetric jet
D	=	nozzle exit diameter
f	=	normalized axial velocity function in the momentum integral
G_θ	=	axial component of angular momentum flux
g	=	normalized azimuthal velocity function in the momentum integral
L	=	axial length scale
M_x	=	axial momentum flux
m_x	=	mass flux in the axial direction
N_{eff}	=	number of effectively independent samples
R	=	nozzle exit radius
Re	=	Reynolds number based on the jet diameter
S	=	swirl number, $G_\theta/M_x R$
U, V, W	=	mean axial, radial, and tangential velocity components in the flow
U_0	=	average exit axial velocity
u, v, w	=	fluctuating axial radial and azimuthal velocity component
x, r, θ	=	cylindrical coordinate system
x_o	=	virtual origin for self-preserving axisymmetric jet
α	=	thermal diffusivity
β	=	volumetric thermal expansion coefficient
$\delta_{1/2}$	=	jet half-width
$\epsilon^2_{\psi_N}$	=	relative statistical error of estimator ψ_N
ε_v	=	viscous dissipation
η	=	normalized radial coordinate in the momentum integral

Subscripts

c	=	centerline
max	=	maximum value
o	=	jet, nozzle exit condition
rms	=	root mean square value
∞	=	freestream or ambient conditions
$*$	=	scaled property

I. Introduction

TURBULENT jets have continued to interest researchers for many years, both because of their numerous applications and their importance to our fundamental understanding of turbulence. Jet flows with swirl are of particular interest, especially in combustion, and many experimental and theoretical studies have tried to address the questions of the stability and dependency on the initial condition of jet flow. But even the nonswirling axisymmetric jet has proven to be a considerable challenge to researchers, and only recently has the role of upstream conditions and downstream similarity been fully recognized [1–3]. Only with this recognition has it become possible to sort out the apparently conflicting results for even the single-point turbulence statistics [4,5].

Swirling jets add to the interest of this class of flows because swirl can be considered as a significant change in the jet flow's initial conditions. Farokhi et al. [6] and Gilchrist and Naughton [7] investigated the effect of swirl on the near-field flow of an axisymmetric jet and showed that moderate swirl (below vortex breakdown) enhances the growth rate and mixing, compared with those of a nonswirling jet. The latter presented evidence that the enhanced growth rates persisted to 20 diameters downstream of the jet exit, even though the swirl had decayed to a point at which it was barely detectable [7]. Such changes in the flow characteristics in the near field would suggest that some turbulence structure of the swirling jet must persist far downstream.

Presented as Paper 3367 at the 36th AIAA Fluid Dynamics Conference and Exhibit, San Francisco, California, 5–8 June 2006; received 21 June 2007; revision received 1 April 2008; accepted for publication 15 April 2008.

*Ph.D. Student, Department of Applied Mechanics. Member AIAA.
†Professor, Department of Applied Mechanics. Associate Fellow AIAA.
‡Associate Professor, Mechanical Engineering Department. Associate Fellow AIAA.

Although swirling jets have been studied for a long time, detailed measurements of the far-field flow under carefully controlled conditions are lacking. The objective of the present study is to make such measurements in the jet far field using laser Doppler anemometry (LDA) to complement our existing knowledge of these flows. The LDA data acquired here are used to assess the characteristics of the swirling jet in the far field and to compare these results with those in the near field. In contrast to the earlier studies of the near field, the present results for the far jet show a linear growth rate for the far field of swirling jet that is the same as for the nonswirling jet. Moreover, if the statistical moments are properly scaled using the rates at which momentum and mass are added at the source, there appears to be no effect of swirl in the far field other than to move the virtual origin of the flow. The overall findings substantiate the theoretical analysis of Ewing [8], who used equilibrium similarity considerations to argue that the effects of swirl on the asymptotic jet should be negligible.

In the following sections, the implications of the governing equations and the similarity results are reviewed. It is argued that the swirl introduces another length scale into the problem, with the consequence that the swirl number is a ratio of length scales. Next, the experimental facility and experiments are described and the data are presented. Finally, the implications of the similarity analysis on the results are considered.

II. Implications of the Governing Equations

A. Basic Scaling Parameters

The basic equations have been carefully reconsidered recently by Ewing [8] and Shiri [9]. Of primary concern for this paper are the two fundamental integrals of the Reynolds-averaged Navier–Stokes equations for the fully developed asymptotic turbulent swirling jet. The first is M_x, which is the total rate of transfer of kinematic linear momentum across any downstream plane (say, at location x). At high Reynolds numbers and in the absence of an external flow, this reduces to [8]

$$M_x = 2\pi \int_0^\infty \left[U^2 - \frac{W^2}{2} + \langle u^2 \rangle - \frac{\langle v^2 \rangle + \langle w^2 \rangle}{2} \right] r \, \mathrm{d}r \qquad (1)$$

Moreover, because there are no net forces other than pressure [which is accounted for in Eq. (1)] acting on any control volume containing this plane and the exit plane of the jet, M_x must remain equal to its source value M_o at all downstream positions x [5].

The second fundamental parameter G_θ is that rate at which kinematic angular momentum is swept across any downstream plane. From integration of the angular momentum equation with the same preceding assumptions, this reduces to [8]

$$G_\theta = 2\pi \int_0^\infty [UW + \langle uw \rangle] r^2 \, \mathrm{d}r \qquad (2)$$

Like the linear momentum, G_θ should remain constant at its source value G_o, because in an infinite environment, there are no torques acting on any control volume containing the source plane and any plane that cuts perpendicularly through the jet axis.

B. Effect of Mass Addition at the Source

A third integral provides the rate at which volume (kinematic mass) is swept across any downstream plane

$$m_x = 2\pi \int_0^\infty U r \, \mathrm{d}r \qquad (3)$$

Unlike M_x and G_θ, m_x is not constant at the rate at which kinematic mass is being added at the source, m_o, because mass is being continually entrained by the jet. Nonetheless, in nonswirling jets, m_o (together with M_o) sets the virtual origin of the jet [1], because it imposes a length scale D_* at the exit plane. D_* is the effective diameter defined by

$$D_* = \sqrt{\frac{m_o^2}{M_o}} \qquad (4)$$

In fact, it is the ratio of the axial distance x to this length scale that measures the evolution of the near jet into the far jet. In particular, it is only when $x \gg D_*$ that the asymptotic free jet can be reached. Or, said another way, only when the mass entrained by the turbulence overwhelms that added at the source close the jet is the asymptotic state attained.

The addition of mass at the source also introduces a velocity scale U_* into the problem. U_* is defined by

$$U_* = \frac{M_0}{m_0} \qquad (5)$$

Both D_* and U_* can simply be replaced by the exit diameter D and exit velocity U_o if (and only if) the exit profile has top-hat form (i.e., uniform velocity across the exit plane). This is easy to see, because in the top-hat case,

$$D_* = \frac{\sqrt{\pi}}{2} D \qquad (6)$$

$$U_* = U_0 \qquad (7)$$

Much confusion in the history of the study of turbulent jets has resulted from the failure to recognize the importance of using D_* and U_* if the exit profile is not a top hat. And often, the alleged effects of source conditions can be eliminated with proper scaling. As will be shown subsequently, proper scaling becomes even more important when swirl is introduced, because the effect of G_o is to introduce yet another length scale into the problem.

C. Role of Swirl

It is easy to show that the addition of both linear and angular momentum imposes another length scale, L_*, onto the flow, even without mass addition at the source (i.e., point sources of linear and angular momentum). L_* can be defined as

$$L_* = \frac{G_o}{M_o} \qquad (8)$$

It is immediately obvious that if mass is also added, then another length-scale ratio, the so-called swirl number, can be defined as

$$S_* = \frac{G_o}{M_o D_*} \sqrt{\pi} \qquad (9)$$

Note that the factor of $\sqrt{\pi}$ has been inserted into Eq. (9) to make it reduce to the usual definition for top-hat exit profiles (which seldom can be achieved when swirl is present); that is,

$$S = \frac{2G_o}{M_o D} = \frac{L_*}{D_*} \sqrt{\pi} \qquad (10)$$

Clearly we should expect L_* to replace D_* as the length scale governing downstream behavior only when the swirl number is large (in much the same manner that x replaces D_* for the far nonswirling jet). Because (as will be reviewed subsequently) the effect of angular momentum on the flow diminishes as the flow evolves downstream, at low swirl numbers, L_* will provide an indication of a measure of, at most, a change in the virtual origin of the asymptotic swirling jet.

D. Equilibrium Similarity Implications for the Far Swirling Jet

The similarity of the asymptotic swirling axisymmetric jet has recently been reconsidered [8,9]. The results can be summarized as follows.

1) The profiles of mean streamwise velocity and turbulence normal stresses can be described by single length and velocity scales. The convenient choices (and those used to scale the data in this paper) are the centerline velocity U_c and the velocity half-width $\delta_{1/2}$

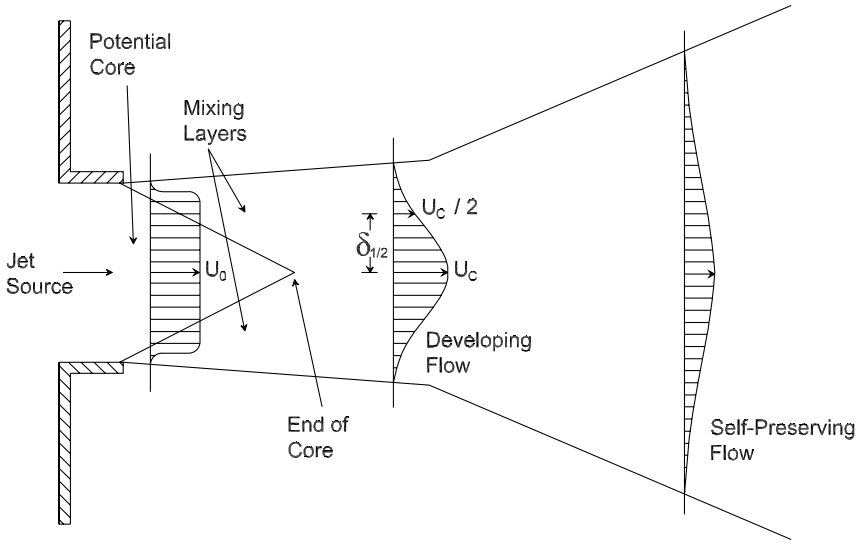

Fig. 1 Schematic of the early development of a jet.

(defined as the distance from the centerline to the point at which the mean velocity falls to half its centerline value, shown in Fig. 1). Thus, the normalized radial coordinate is $\eta = r/\delta_{1/2}$, exactly like the nonswirling jet.

2) The spreading rate of the asymptotic jet is linear; that is,

$$\delta_{1/2} = A(x - x_o) \tag{11}$$

where x_o is a virtual origin that can depend on the Reynolds number and swirl number. The coefficient A (or $d\delta_{1/2}/dx$) can (in principle, at least) depend on the jet exit conditions. Both sides can be normalized by D_*, but normalization by D introduces a dependence on the exit profile (which can be nonuniform with swirl). Note that if done rigorously, the result of Eq. (11) is not particularly straightforward to obtain, but follows from a detailed consideration of the Reynolds shear stress equations and the behavior of the dissipation [1,5].

3) The Reynolds shear stress $\langle uw \rangle$ scales with $U_c^2\, \mathrm{d}\delta_{1/2}/\mathrm{d}x$. The linear growth of the far jet implied by Eq. (11) means that the factor of $\mathrm{d}\delta_{1/2}/\mathrm{d}x$ is constant, and so these moments scale the same as the turbulence intensities. However, it should be noted that the dependence of the coefficient on upstream conditions means that scaled profiles may differ from experiment to experiment.

4) From the conservation of linear momentum [Eq. (1)], it follows immediately that the mean centerline velocity falls asymptotically inversely with increasing $\delta_{1/2}$. Although this is well known [1,5], it is instructive to briefly review the reasons, because similar considerations apply to the angular momentum considered subsequently. First, ignore for the moment the swirl and turbulence contributions, and substitute the similarity profile for the mean velocity into Eq. (1) to obtain

$$M_x = [U_c^2 \delta_{1/2}^2] 2\pi \int_0^\infty f^2 \eta \, \mathrm{d}\eta \tag{12}$$

where $\eta = r/\delta_{1/2}$ and $f = U/U_c$. Because the integrand depends only on the similarity variable η that is integrated over the entire domain, all of the x dependence on the right-hand side is in the square-bracketed term. But the left-hand side is equal to a constant because $M_x = M_o$. Therefore, U_c must be inversely proportional to $\delta_{1/2}$; that is,

$$U_c \propto \delta_{1/2}^{-1} \tag{13}$$

Inclusion of the turbulence terms only modifies the constant of proportionality, because they too can be shown to scale with U_c^2. The swirl contribution (from the radial pressure gradient), $W^2/2$ will be shown subsequently to vanish downstream relative to the other terms, and so the effect of its omission decreases with distance. Combining Eqs. (12) and (13) with the linear growth rate of Eq. (11) implies that

$$U_c = B_u \frac{M_o^{1/2}}{(x - x_o)} \tag{14}$$

where B is a constant. In fact, B and A cannot be independent, but must also be linked to each other and the shape of the profile through Eq. (1). Alternatively, the centerline velocity can be normalized by U_*:

$$\frac{U_*}{U_c} = \frac{1}{B_u}\left[\frac{x}{D_*} - \frac{x_0}{D_*}\right] \tag{15}$$

Note that U_o can be also used if the exit profile is top hat, but if it is not, this introduces an artificial dependence on jet exit conditions.

5) The mean azimuthal (or swirl) velocity component scales with its maximum value at any cross section, $W_{\max}$, and falls off as the inverse square of $\delta_{1/2}$ (or $x - x_o$). This is a surprising result (originally shown by Ewing [8]), but can be seen immediately by substituting similarity profiles for the mean velocity [say, $U/U_c = f(\eta)$ and $W/W_{\max} = g(\eta)$] into the angular momentum integral of Eq. (2). Because $\langle uw \rangle$ is negligible, the result is

$$G_x = [U_c W_{\max} \delta_{1/2}^3] 2\pi \int_0^\infty f g \eta^2 \, \mathrm{d}\eta \tag{16}$$

The integral in similarity variables can, at most, depend on the exit conditions and is independent of x. Also, the left-hand side is constant because conservation of angular momentum requires that $G_x = G_o$. Using Eq. (14) implies

$$W_{\max} \propto [U_c \delta_{1/2}^3]^{-1} \propto [\delta_{1/2}]^{-2} \tag{17}$$

It follows immediately from Eq. (11) that the swirl velocity $W_{\max}$ falls off inversely with the square of the downstream distance. Combining Eq. (16) with Eqs. (11) and (14) yields

$$W_{\max} = C \frac{G_o}{M_o^{1/2}(x - x_o)^2} \tag{18}$$

where C is a constant (at most, dependent on the jet exit conditions). Note that just as A and B are linked by the linear momentum integral, C is linked to both by the angular momentum integral.

Because the mean velocity falls off only inversely with distance, but the swirl falls off as inversely with the square of distance, the swirl should appear to die off. This is exactly what was noted in the

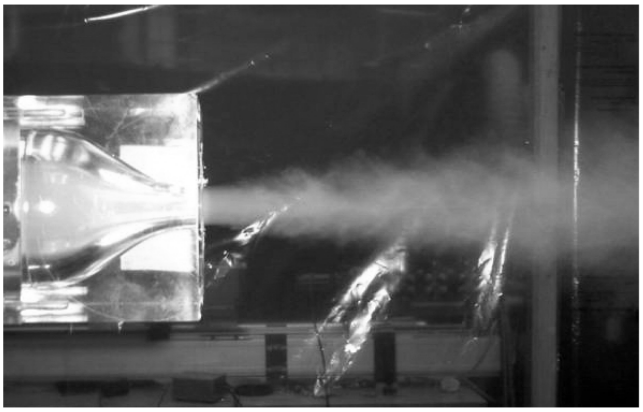

Fig. 2 Photograph of the jet nozzle and exit flow using smoke for visualization.

experiments of Gilchrist and Naughton [7]: the swirl dies off downstream. Moreover, as first pointed out by Ewing [8], this means that the asymptotic swirling jet should behave exactly as a nonswirling jet with, at most, different values of A, B, and C that could in turn depend only on the jet exit conditions. A particular goal of the experiments described subsequently was to test if and how these things happen.

Note that the fact that the swirl appears to die out relative to the streamwise flow does not mean it is gone: angular momentum is still being conserved, it is just being spread over a larger area. As a consequence, the swirl (or azimuthal mean equation) uncouples itself and plays no role in the evolution of the streamwise and radial equations, which behave as though the jet were nonswirling.

III. Experimental Setup

A. Jet Facility

The free jet used in the experiment is shown in Fig. 2. It was a preexisting Turbulence Research Laboratory facility [5] that was modified to produce both axial and tangential velocity at the exit. Two contractions were used to reach the jet exit diameter of 25.4 mm (1 in.). One blower was used to supply axial flow, and six 15-mm injectors connected to a different blower were used to add the swirling component independently. The resulting swirling jets had a solid-body-like swirl distribution at the nozzle exit. As noted by Hussein et al. [5] (see, especially, the Appendix), there can be significant differences between a jet in a confined or semiconfined enclosure and one in an infinite environment, because of the recirculating flow entrained by the jet. The $10 \times 3.5 \times 3.5$ m enclosure was designed to minimize the backflow momentum to at least 100 diameters and also to provide uniform spatial seeding for the LDA measurement. A closed-loop circulation was achieved by placing the blower inlet inside the tent, but far from the jet exit.

B. Laser Doppler Anemometry Method

A two-component laser Doppler anemometry system (Dantec) was used in a backscatter arrangement for the present study. The flow was seeded with an aerosol, and bursts produced by particles passing through the control volume were analyzed by Dantec burst spectrum analyzers. The sampling rate of the LDA system was not fixed, but rather a burst mode was used in which all particles were sampled as they arrived. The particles produced by a Safex fog generator that generates a dense white fog by evaporation and condensation of a water-based fog liquid. The mean droplet size was around 1 μm and a closed-loop circulation of air kept the particle density constant during the measurement. The particle time constant was estimated to be approximately 2.3 μs, which can be compared with the smallest Kolmogorov microtime (at $x/D = 10$) estimated as 160 μs, using the results of Hussein et al. [5]. The most notable effect of the additional swirl velocity component was to reduce the particle concentration near the jet exit at the centerline jet, compared with the nonswirling jet.

C. Statistical Uncertainty

All statistical moments were computed using the residence time weighting [10,11] as employed by Hussein et al. [5]. A fixed sampling period of 200 s was used, and in most locations, the number of samples was at least 40,000 at each point in high-velocity regions and more than 4000 at regions with a velocity less than 1 m/s. The largest estimate of the integral time was 0.25 s, and so the minimum number of effectively independent samples was 400. Thus, the relative statistical error can be estimated as [12]

$$\epsilon^2_{\psi_N} = \frac{1}{N_{\text{eff}}} \frac{\text{var}(\psi_N - \langle\psi\rangle)}{\langle\psi\rangle^2} \tag{19}$$

where ψ is the statistical quantity being estimated and ψ_N is the estimator using N independent estimates. The relative statistical error for the mean streamwise velocity U is estimated to be less than 2.5% (high-velocity regions at the far field of the jet) and, at most, 7% (at low-velocity regions of the jet) for the second-moment statistics. Most problematic for these measurements was the mean swirl velocity W, for which Eq. (19) reduces to

$$\epsilon^2_{W_N} = \frac{1}{N_{\text{eff}}} \frac{\langle w^2\rangle}{W^2} \tag{20}$$

The mean square azimuthal velocity $\langle w^2\rangle$ is about equal to the other turbulence normal stresses and scales with U_c^2, but the expected value of W drops rapidly with increasing x (as previously noted). Therefore, even if great care is taken in aligning the optical system to enable accurate measurement of W, statistical errors greatly complicate its determination. At the farthest downstream location, the relative statistical error of the measurement of $W_{\max}$ was estimated to be 23%. Note that similar problems occur for the measurement of the radial component, but these can be overcome by computing V from U using the continuity equation (at least if similarity is established).

D. Test Cases

Surveys were made at several locations downstream ($x/D = 5$, 10, 20, 25, 30, 35, 40, and 50) and also at the jet exit. The latter measurements were necessary to quantify the rates at which mass, momentum, and angular momentum were added to the flow. These were crucial in scaling the data and in establishing the swirl number of each for the flow. As will be illustrated subsequently, the exit axial velocity profiles for the two flows differed slightly from the near top hat of the nonswirling jet. As a consequence, a simple scaling with the source velocity was neither possible nor desirable.

Mean velocities in the axial and azimuthal directions at the exit of the jet were measured to calculate the swirl strength and Reynolds number of the jet flow. A list of the test cases is provided in Table 1, in which each case has been listed by its swirl strength S. The axial and tangential velocities have been adjusted to produce three cases of flow at the same Reynolds number value of $Re \approx 45,000$.

Table 1 Test cases for the present study

Case number	S	$U_{c,0}$, m/s	$W_{\max,0}$, m/s	U_*, m/s	D_*, mm	M_o	m_o	S_*
Case 1	0	26.3	0	25.9	22.7	0.347	0.0268	0
Case 2	0.15	27	6.7	24.8	22.9	0.323	0.0260	0.145
Case 3	0.25	28.4	10	22.9	23.5	0.289	0.0252	0.239

IV. Results

A. Exit Velocity Profiles

The exit velocity profiles for the three cases are shown in Fig. 3. The nonswirling jet has a top-hat axial mean velocity profile at the jet exit. But the swirling jet profiles all exhibit profiles with a peak axial velocity on the centerline. Also, the magnitude of the centerline velocity increases with increasing swirl number. Similar axial profiles have been observed by Gilchrist and Naughton [7] and Farokhi et al. [6]. Panda and McLaughlin [13] also saw this peak and provided an explanation based on vortex tubes becoming spirals.

B. Mean Velocity Profiles in the Far Jet

It is clear from Fig. 3 that the velocity profiles for the swirling jets are not top-hat profiles, nor is the centerline velocity at the exit representative of the exit flow. Therefore, to have a reliable comparison between three different cases, it is necessary to scale the far jet data with the D_* and U_* [defined by Eqs. (4) and (5), respectively]. Figure 4 shows the mean axial velocity profiles for all three cases ($S = 0$, 0.15, and 0.25) and all downstream positions ($x/D_* = 20$, 25, 30, 35, 40, and 50). The mean velocity has been normalized by its centerline value U_c, and the radial coordinate has been normalized by the jet half-width $\delta_{1/2}$ (determined as described in the next section). In all three cases, the normalized velocities show collapse of the data for all cross sections in the far-field region of the jet. Moreover, there is very little (if any) difference from one set of data to the next. Both of these observations are consistent with the theory presented earlier that the far asymptotic swirling jet should appear to be independent of swirl.

C. Variation of U_c and $\delta_{1/2}$ with x

The jet velocity half-width is defined as the distance between the centerline and the location where the axial velocity drops to half of the centerline velocity. To calculate these values for each curve, the following empirical jet profile was fitted to each profile [14]:

$$\frac{U}{U_c} = \sec h^2\left(a\frac{r}{x}\right) \tag{21}$$

The results are shown in Fig. 5. The solid lines drawn on the figure for $S = 0$ and 0.15 are regression fits of Eq. (11) with both sides divided by D_*. For both, the slope of the curves A is 0.093 and the virtual origin is at $x_o = 0.75$. The value of A is very close to the value of $A = 0.94$ in the nonswirling jet of Hussein et al. [5]. The virtual origin, however, is closer to the exit plane, undoubtedly reflecting the differences in the way the flows were generated.

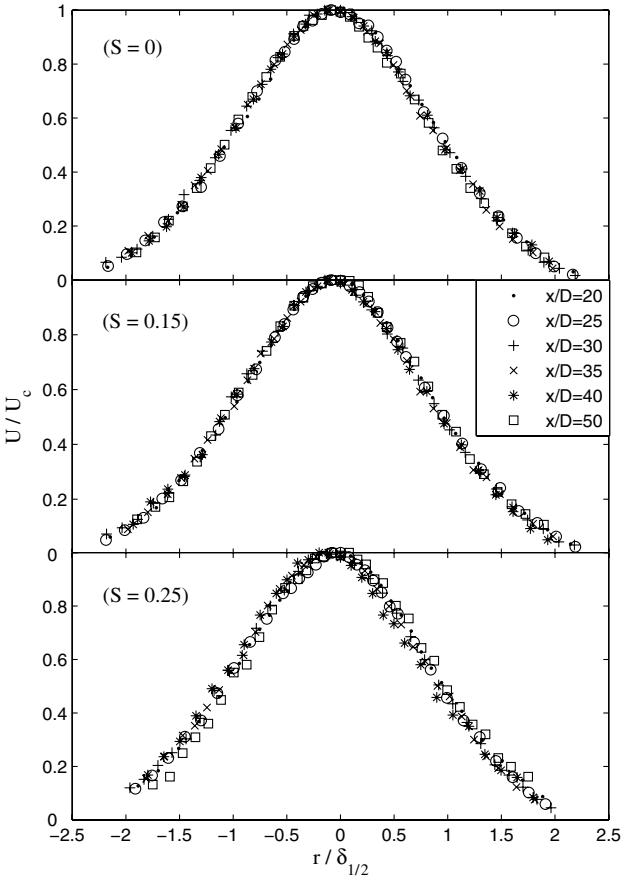

Fig. 4 Mean streamwise velocity at different axial positions for three different swirl numbers $S = 0$, 0.15, and 0.25. The profiles have been normalized by the local mean centerline velocity U_c and the half-width $\delta_{1/2}$.

The same regression fit to the $S = 0.25$ case yields 0.96 and −3.2, respectively. Drawn instead on the $S = 0.25$ data is a solid line with the same slope as for the $S = 0$ and 0.15 cases, which clearly provides an almost equally good fit to the data. This suggests strongly that there is really no statistically significant difference in the spreading rate for the three swirl values. There is most certainly, however, a change in virtual origin, which even with the modified curve fit has moved from the zero and low swirl values to $x_o = -2.9$. The fact that there are no differences at all when the flow has a low

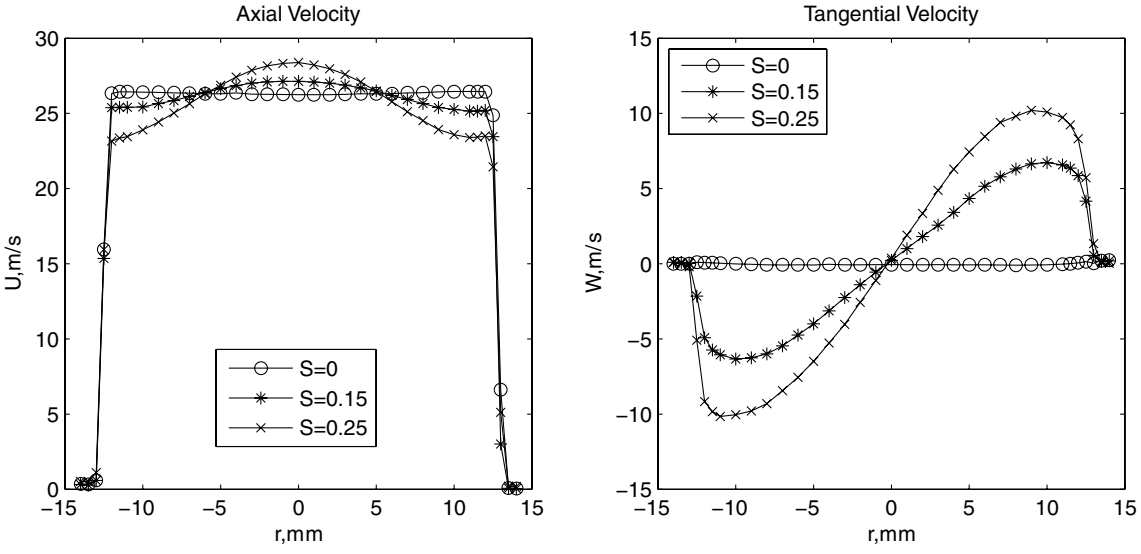

Fig. 3 Axial and tangential mean velocity profiles at the jet exit for three different swirl numbers.

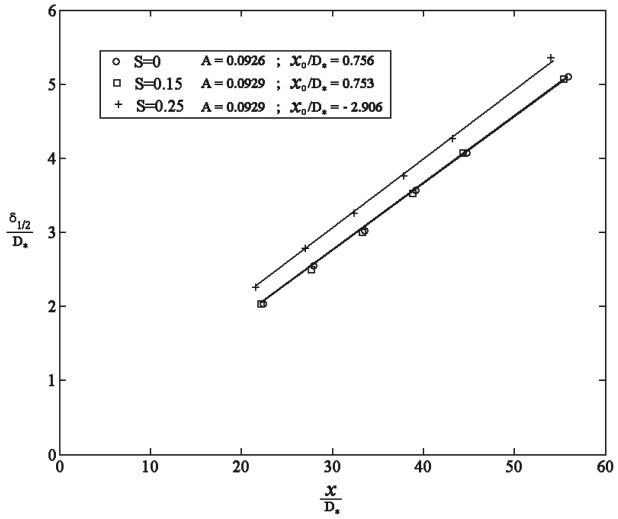

Fig. 5 Streamwise variation of the velocity profile half-width.

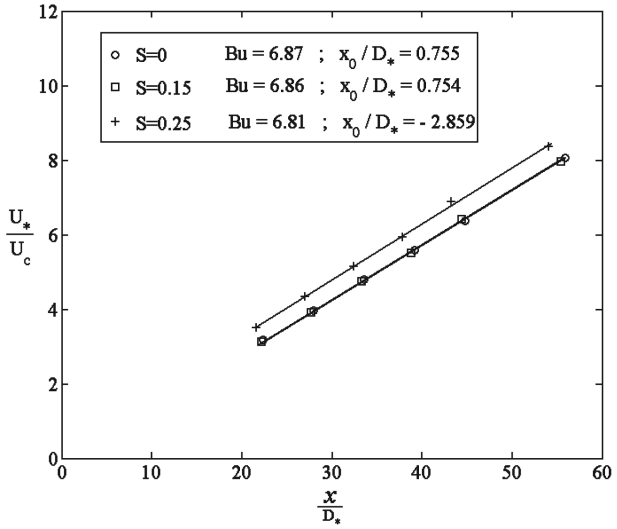

Fig. 6 Streamwise variation of centerline mean velocity.

swirl number is consistent with the earlier observations that the swirl number must exceed certain value (between $S = 0.15$ and 0.25) for any effect to be noticed on the near field [7].

The mean streamwise centerline velocity is plotted as a function of downstream location in Fig. 6 in the region where the jet can be assumed to be self-preserving ($x/D_* > 20$). The solid lines shown are regression fits of Eq. (15). Because the local centerline velocity appears in the denominator of the ordinate, the $1/(x - x_o)$ decay rate is manifested as a straight line in the figure, the slope of which is $1/B_u$. For the $S = 0$ and 0.15 jets, the values of B_u are nearly identical at 6.87 and 6.86, respectively, and the virtual origins are the same at $x_o = 0.75$. (Note that the virtual origins are the same as for the curve fits to $\delta_{1/2}$, *as they must be*.) These values are slightly higher than the equivalent value from Hussein et al. [5] that, when converted from D_* to D, yields $B_u = 6.55$.

The regression fit to the data for the $S = 0.25$ case yields a somewhat smaller value of $B_u = 6.61$ case, with a virtual origin of -1.65. But as with the preceding half-width plots, a curve can be drawn on this data with the same slope as the others; only the virtual origin need be modified.

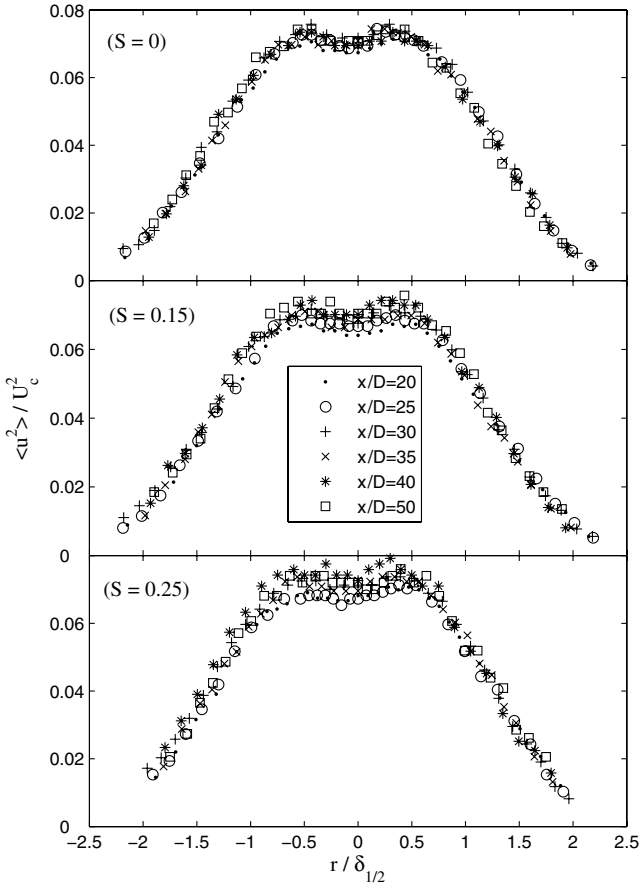

a) Normalized axial normal stress

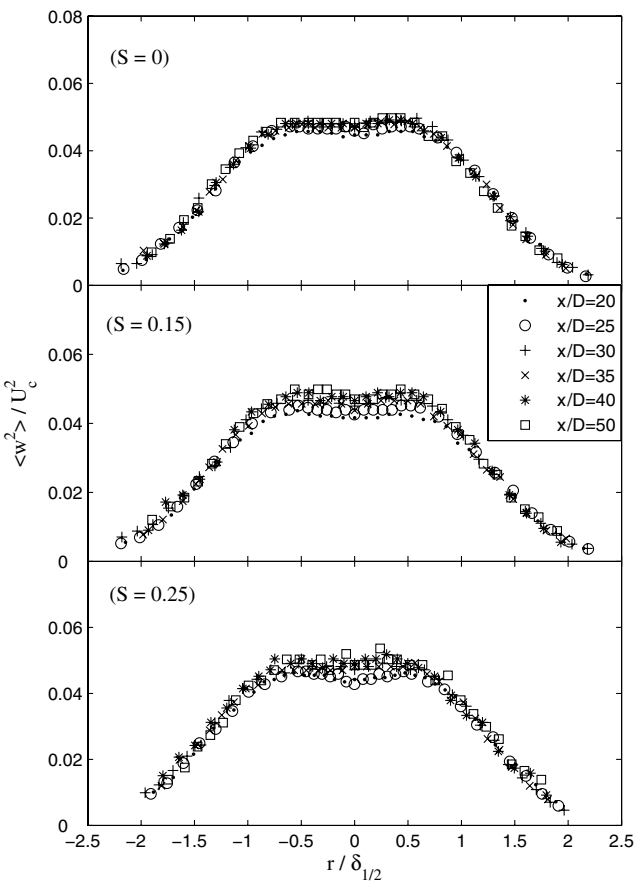

b) Normalized tangential normal stress

Fig. 7 Normalized plots of u'/U_c and w'/U_c for all positions for different cases $S = 0$, 0.15, and 0.25.

Therefore, the data as plotted behave according to the expected linear functions of the axial distance. To within the statistical error, there is no change on either the spreading rate or the rate at which the centerline velocity decays, other than the change in virtual origin for the $S = 0.25$ case. The fact that this shift occurs for $S > 0.2$ is consistent with the changes observed by others [7,15].

Before leaving this section, it should be noted that all values of the preceding chosen parameters satisfy the constraint imposed by the similarity form of the linear momentum conservation expressed by Eq. (13). For all three data sets, $A^2B_u^2 = 0.405 \pm 1\%$. This, together with the collapse of the profiles in similarity variables, is a necessary consequence of momentum conservation.

D. Turbulence Quantities

Figure 7 shows the distribution of two components of turbulence intensity available from this experiment: $u_{\rm rms}/U_c$ and $w_{\rm rms}/U_c$. Unlike mean streamwise velocity profiles, in these profiles, there are some variations in the core for swirling cases for $x/D < 30$, which might indicate that the swirling cases are collapsing slower. For the region further than $x/D = 30$, the second moments are consistent with all previous jet measurements [4,5] and, in fact, the swirl seems to have had no effect at all on the second moments. This is consistent with the theoretical prediction of Ewing [8] and confirms the equilibrium similarity approach, at least for the second moments.

Figure 8 plots the correlation coefficient between the two fluctuating velocity components (i.e., $\langle uw\rangle/u_{\rm rms}w_{\rm rms}$). This correlation coefficient is zero to within the statistical and measurement error. This is consistent with the expected azimuthal homogeneity of the flow and confirms the passive role of the mean equation for W.

V. Vanishing Swirl Velocity

As noted earlier, the measurement of W, the mean swirl component of velocity, was the most difficult part of the experiment. Because it is almost 2 orders of magnitude less than the streamwise mean velocity at the locations of interest, even fractions-of-a-degree difference in the alignment of the laser beams introduces significant errors. Also, because of the very low value of W compared with $\langle w^2\rangle$, there is considerable scatter in the results, purely because of the statistical error. Nonetheless, by trying to account for the small offset near the origin and fairing curves through points near the local maxima, it was possible to make an estimate of $W_{\rm max}$ for each of the two values of S.

From conservation of angular momentum and equilibrium similarity it was argued that $W_{\rm max}$ is described by Eq. (18) and falls off with increasing x as $1/(x - x_o)^2$. Because U_c [described by Eq. (14)] falls as only $1/(x - x_o)$, then $U_c/W_{\rm max} \propto (x - x_o)$. If it is argued that all of the integrals in similarity variables have constant values (because the normalized profiles are independent of x), the values of C (and B) should be independent of swirl. It follows immediately that the slope of $U_c/W_{\rm max}$ should be proportional to M_o/G_o; that is,

$$\frac{U_c}{W_{\rm max}} = \frac{C}{B}\frac{M_o}{G_o}(x - x_o), = \frac{C}{B}S_*^{-1}\left[\frac{(x - x_o)}{D_*}\right] \tag{22}$$

Thus, the higher the swirl number, the farther downstream for the swirl to die off relative to the jet centerline velocity. Alternatively, from the definition of L_* in Eq. (8), it follows immediately that

$$\frac{U_c}{W_{\rm max}} = \frac{B}{C}\frac{(x - x_o)}{L_*} \tag{23}$$

Thus, the role of L_* as a second length scale is clear: it measures the distance for the swirl mean velocity to die off.

Figure 9 plots $U_c/W_{\rm max}$ versus x/D_*. The fitted lines in the figure use the same virtual origins obtained for the $S = 0.15$ and 0.25 cases (i.e., $x_o = 0.75$ and -2.9, respectively). From the considerations of the preceding paragraph, the ratio of the slopes of the two plots should be equal to the ratio of the values of G_o/M_o itself, which is

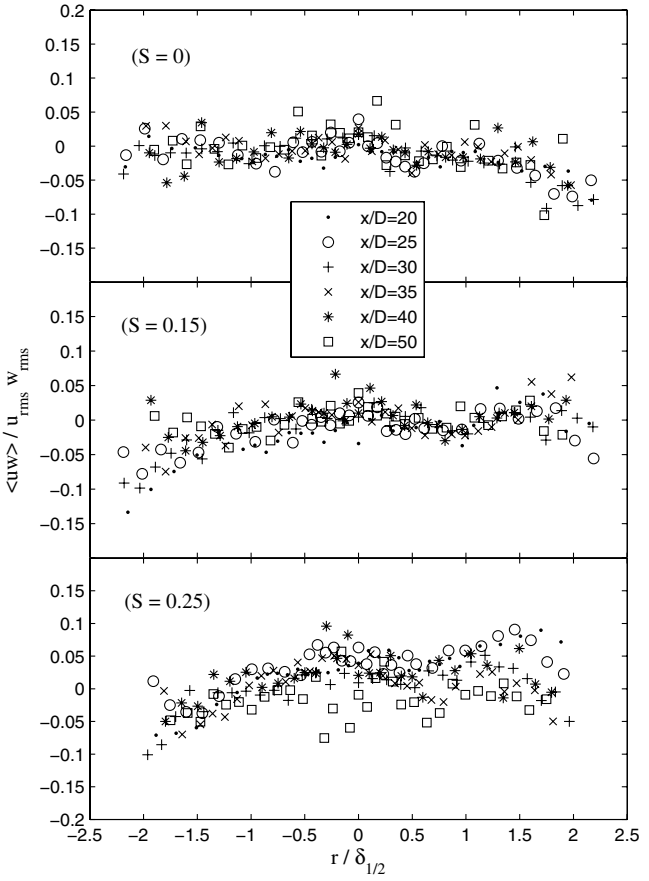

Fig. 8 Normalized plots of $\langle uw\rangle/u_{\rm rms}w_{\rm rms}$ for all positions for different cases: a) $S = 0$, b) $S = 0.15$, and c) $S = 0.25$.

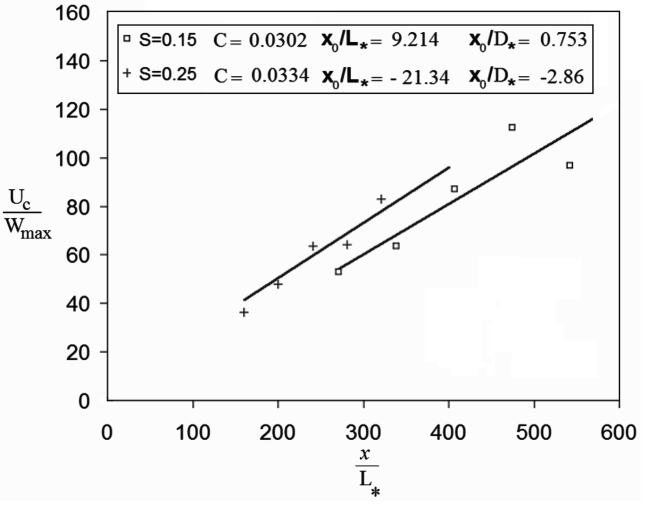

Fig. 9 $U_c/W_{\rm max}$ versus x/D_* using the same virtual origins as before; that is, for $S = 0.15, x_o = 0.75$ and for $S = 0.25, x_o = 2.9$.

0.59. The individual slopes are 0.395 and 0.593, respectively, the ratio of which is 0.66. Thus, in spite of the considerable scatter in the measurement of W and the data presented in Fig. 9, the overall inferences from them are, at the very least, consistent with Ewing's theory [8].

VI. Conclusions

The far field of an incompressible swirling jet was studied using two-dimensional laser Doppler anemometry. Three pairs of symmetric injectors were used to produce weak-to-moderate swirling jets. Velocity profiles of the mean and fluctuating streamwise and

azimuthal velocity components were measured in jets with two levels of swirl ($S = 0.15$ and 0.25) at axial locations up to 50 jet exit diameters. The velocity and turbulence intensity profiles, centerline decay, and growth rates for the various swirling jets were compared with those obtained in the same facility without swirl ($S = 0$). The mean velocity and turbulence intensities collapsed to the same profiles when scaled with the jet centerline velocity and half-width. Thus, by contrast with previous observations for the near jet [7,15], there was no observable effect on the properly scaled far jet for the $S = 0.15$ case. The results were virtually identical to the nonswirling jet. For the $S = 0.25$ case, the only statistically significant effect was a shift in the virtual origin (from $x/D_* = 0.75$ to -2.9), indicating a more rapid initial spread rate that relates to jet growth in far-field.

The recent predictions of equilibrium similarity theory [8] were found to be in excellent agreement with the experimental results. In particular, the mean azimuthal component of velocity falls off as the inverse square of the downstream distance. By contrast, the mean streamwise velocity and turbulence intensities fall off with simply the inverse of the downstream distance. As a consequence, the mean azimuthal equation uncouples from the rest, and so the asymptotic swirling jet behaves like the nonswirling jet. A second length scale, L_*, defined from the rates at which momentum and angular momentum are added at the source, characterizes the distance that is required for the swirl to become negligible.

Acknowledgments

These measurements were initiated at Chalmers University of Technology while J. Naughton was a visiting professor at the Turbulence Research Laboratory. The authors are especially grateful to T. Gunnar Johansson for his helpful advice and counsel. D. Ewing also provided useful insight and comments.

References

[1] George, W., "The Self-Preservation of Turbulent Flows and Its Relation to Initial Conditions and Coherent Structures," *Advances in Turbulence*, edited by W. George and R. Arndt, Springer, New York, 1989, pp. 39–73.

[2] Mi, J., Nobes, D., and Nathan, G., "Influence of Jet Exit Condition on the Passive Scalar Field of an Axisymmetric Free Jet," *Journal of Fluid Mechanics*, Vol. 432, 2001, pp. 91–125.

[3] Cater, J., and Soria, J., "The Evolution of Round Zero-Net-Mass-Flux Jets," *Journal of Fluid Mechanics*, Vol. 472, 2002, pp. 167–200. doi:10.1017/S0022112002002264

[4] Panchapakesan, N., and Lumley, J., "Turbulence Measurements in Axisymmetric Jets of Air and Helium, Part 1: Air Jet," *Journal of Fluid Mechanics*, Vol. 246, 1993, pp. 197–223. doi:10.1017/S0022112093000096

[5] Hussein, H., Capp, S., and George, W., "Velocity Measurements in a High-Reynolds-Number, Momentum-Conserving, Axisymmetric, Turbulent Jet," *Journal of Fluid Mechanics*, Vol. 258, 1994, pp. 31–75. doi:10.1017/S002211209400323X

[6] Farokhi, S., Taghavi, R., and Rice, E., "Effect of Initial Swirl Distribution on the Evolution of a Turbulent Jet," *AIAA Journal*, Vol. 27, No. 6, 1989, pp. 700–706.

[7] Gilchrist, R., and Naughton, J., "Experimental Study of Incompressible Jets with Different Initial Swirl Distributions: Mean Results," *AIAA Journal*, Vol. 43, No. 4, 2005, pp. 741–751. doi:10.2514/1.3295

[8] Ewing, D., "Decay of Round Turbulent Jets with Swirl," *Proceedings of the 4th International Symposium on Engineering Turbulence Modeling and Experiments*, Elsevier, New York, 1999.

[9] Shiri, A., *Turbulent Shear Flow Experiments: Design of Natural Convection Rig and LDA Measurement in Swirling Jets*, Chalmers Univ. of Technology, Götebory, Sweden, June 2006.

[10] Buchhave, P., George, W. K., and Lumley, J. L., "The Measurement of Turbulence with the Laser-Doppler Anemometer," *Annual Review of Fluid Mechanics*, edited by V. Dyke, Wehausen, and Lumley, Vol. 11, Academic Press, New York, 1979, pp. 443–503.

[11] George, W. K., "Quantitative Measurement With the Burst-Mode Laser Doppler Anemometer," *Experimental Thermal and Fluid Science*, Vol. 1, 1988, pp. 29–40. doi:10.1016/0894-1777(88)90045-3

[12] George, W. K., Beuther, P. D., and Lumley, J. L., "Processing of Random Signals," *Proceedings of the Dynamic Flow Conference*, Disa Electronics, Skovlunde Denmark, 1978, pp. 757–800.

[13] Panda, J., and McLaughlin, D., "Experiments on the Instabilities of a Swirling Jet," *Physics of Fluids*, Vol. 6, No. 1, 1994, pp. 263–276. doi:10.1063/1.868074

[14] White, F. M., *Viscous Fluid Flow*, 2nd ed., McGraw–Hill, New York, 1991.

[15] Chigier, N., and Chervinsky, A., "Experimental Investigation of Swirling Vortex Motion in Jets," *TAE Report*, June 1966, p. 53.

R. Lucht
Associate Editor